Thermodynamic and transport studies of the ferromagnetic filled skutterudite compound $PrFe_4As_{12}$

T. A. Sayles, W. M. Yuhasz, J. Paglione, T. Yanagisawa, J. R. Jeffries, and M. B. Maple
Department of Physics and Institute for Pure and Applied Physical Sciences, University of California at San Diego, La Jolla, California 92093, USA

Z. Henkie, A. Pietraszko, T. Cichorek, and R. Wawryk
Institute of Low Temperature and Structure Research, Polish Academy of Sciences, 50-950 Wrocław, Poland

Y. Nemoto and T. Goto
Graduate School of Science and Technology, Niigata University, Niigata 950-2181, Japan
(Received 9 August 2007; revised manuscript received 27 February 2008; published 29 April 2008)

A variety of thermodynamic and transport measurements were made on high-quality single crystals of the Pr-based filled skutterudite compound $PrFe_4As_{12}$. Abrupt features in magnetization, ac susceptibility, specific heat, resistivity, thermoelectric power, and ultrasonic velocity reveal the onset of long range ferromagnetic order below $\Theta_C = 18$ K. The low-temperature magnetic susceptibility is characterized by a Curie–Weiss law with an effective moment of $3.52\mu_B$/f.u. and a saturation magnetization of $2.3\mu_B$/f.u., which is consistent with a magnetic Γ_5 triplet ground state. A gaplike reduction of the large electronic specific heat coefficient of 340 mJ/mol K^2 and several other features point to a strongly correlated electron behavior that is likely coupled to a change in magnetic and/or structural order near $T^* \simeq 12$ K. Furthermore, this complex magnetic state is found to be strongly field dependent, as evidenced by a change in the easy axis at low fields and an additional contribution to thermal conductivity appearing only at high fields.

DOI: 10.1103/PhysRevB.77.144432 PACS number(s): 75.50.Bb, 75.50.Cc, 75.20.Hr, 65.40.G−

I. INTRODUCTION

The AT_4X_{12} family of filled skutterudites—where A is an alkali metal, an alkaline earth, a lanthanide, or an actinide; T is Fe, Ru, or Os; and X is P, As, or Sb—hosts a variety of strongly correlated electron phenomena, which include both conventional and unconventional superconductivities, magnetic and quadrupolar orderings, metal-insulator transitions, Kondo phenomena, heavy-fermion behavior, and non-Fermi liquid behavior.[1,2] Such exotic physical properties readily arise in the A=Pr series of compounds due to both significant hybridization between the localized Pr $4f$ and conduction electron states and splitting of Hund's rule ground state of the Pr^{3+} ion by the crystalline electric field (CEF).[3] An example of this diversity is seen in $PrFe_4P_{12}$, which undergoes a transition to an antiferroquadrupolar (AFQ) state at 6.5 K; applying a magnetic field suppresses the AFQ order and reveals the formation of a heavy Fermi liquid state above a quadrupolar quantum critical point in this compound.[4–6] Currently, one of the most interesting Pr-based filled skutterudites is $PrOs_4Sb_{12}$, i.e., the first Pr-based heavy-fermion superconductor.[7–9] This extraordinary material enters an unconventional superconducting state below $T_c = 1.85$ K, which breaks time reversal symmetry,[10] appears to consist of several distinct superconducting phases,[9,11,12] and may possess point nodes in the energy gap.[11] Furthermore, for fields between 4.5 and 16 T and for $T \leq 1$ K, an AFQ ordered phase was also observed in $PrOs_4Sb_{12}$.[13,14]

While a great deal of research has been performed on Pr-based filled skutterudite phosphides and antimonides, there have been only a few investigations of Pr-based filled skutterudite arsenides. Although the PrT_4As_{12} (T=Fe, Ru, and Os) compounds were all originally synthesized and their lattice parameters were measured by Braun and Jeitschko,[15] only two members of the series have had other physical properties studied; $PrRu_4As_{12}$ was found to be a conventional superconductor with $T_c \approx 2.4$ K,[16–18] and $PrOs_4As_{12}$ was shown to possess multiple low-temperature ordered phases.[19,20] In this paper, the results of an investigation of the physical properties of newly synthesized, high-quality single crystals of $PrFe_4As_{12}$ are reported. A variety of thermodynamic and transport properties were measured, which probe the electronic, magnetic, and structural characteristics of this material in an effort to help elucidate the strongly correlated electron phenomena that are exhibited by Pr-based skutterudite systems. $PrFe_4As_{12}$ is found to ferromagnetically order below a Curie temperature $\Theta_C = 18$ K and to display a number of anomalies in physical properties at lower temperatures.

II. EXPERIMENTAL DETAILS

Single crystals of $PrFe_4As_{12}$ were grown from elements with purities of ≥99.9% by using a molten metal flux method at high temperature and pressure, the details of which will be reported elsewhere.[21] After removing the majority of the flux by distillation, $PrFe_4As_{12}$ single crystals of an isometric form with dimensions of up to ~1.7 mm were collected and etched in HCl acid to remove any impurity phases from the surfaces. X-ray powder diffraction measurements, which are performed with a Rigaku D/MAX B x-ray machine on a powder prepared by grinding several single crystals along with a high purity Si($8N$) standard, did not

reveal any significant impurity phases. The $LaFe_4P_{12}$-type filled skutterudite crystal structure was confirmed for $PrFe_4As_{12}$ by x-ray diffraction on a crystal with a regular octahedral shape and dimensions of $0.16\times0.19\times0.22$ mm^3. A total of 9824 reflections (793 unique, $R_{\text{int}}=0.0791$) were recorded and the structure was resolved by the full matrix least-squares method by using the SHELX-97 program with a final discrepancy factor $R1=0.0372$ [for $I>2\sigma(I)$, $wR2=0.0812$].[22,23] The refinement revealed a lattice parameter of $a=8.310(2)$ Å as well as a full occupancy of the Pr sites.

Measurements of magnetization M as a function of temperature $[M(T)]$ and magnetic field $[M(H)]$ were taken on single crystals by using a Quantum Design magnetic properties measurement system (MPMS) through the temperature range of $1.7\leq T\leq300$ K and in fields of up to 5.5 T. The crystals were oriented for measurements in both the [100] and the [111] high symmetry directions. Measurements of ac susceptibility were performed in a separate MPMS by using an ac field of 0.1 mT that is directed along the [100] crystallographic direction and driven at various frequencies of up to 500 Hz.

The specific heat C of a collection of three single crystals with a total mass of 43.9 mg was measured as a function of temperature T through the range of 650 mK$\leq T\leq$50 K by using a ^{3}He semiadiabatic calorimeter and a standard heat pulse technique.

The electrical resistivity ρ of the single-crystal specimens was measured as a function of temperature and a transverse magnetic field in a ^{4}He cryostat by using an ac resistance bridge and the standard four-wire technique. Measurements of $\rho(T)$ at various applied pressures were performed down to 1 K in a ^{4}He cryostat by using a BeCu piston-cylinder clamp with a 1:1 *n*-pentane:isoamyl alcohol pressure medium. Thermal conductivity κ was measured as a function of temperature by using a standard steady-state one-heater, two-thermometer technique with *in situ* thermometry calibration. Simultaneous measurements of the longitudinal thermoelectric power S were performed by using a nanovoltmeter and were corrected with *in situ* background measurements. Additional thermoelectric power measurements were performed at the Polish Academy of Sciences, which reproduce the results that are obtained at the University of California, San Diego.

Ultrasonic velocity and attenuation in a $PrFe_4As_{12}$ single crystal were measured as a function of temperature by using a phase comparative method at Niigata University in a ^{3}He-evaporation refrigerator, which operates from room temperature to 400 mK. Piezoelectric $LiNbO_3$ transducers on 36° *y* cut and *x* cut, which are bonded to the parallel [100] facets, were used for generating and detecting longitudinal and transverse ultrasonic waves, respectively. The elastic constants C_{11} and C_{44} were obtained for longitudinal ultrasonic waves $\mathbf{k}$(propagation)$\|\mathbf{u}$(polarization)$\|$[100] with a frequency of 109 MHz and for transverse ultrasonic waves $\mathbf{k}\|$[100] and $\mathbf{u}\|$[100] with a frequency of 20 MHz.

III. RESULTS

A. Magnetic susceptibility

Figure 1 presents the inverse dc magnetic susceptibility χ_{dc}^{-1} of a $PrFe_4As_{12}$ single crystal, which is measured in a constant magnetic field of 0.5 T that is oriented along the [100] crystal axis from 2 to 300 K, which is displayed along with a Curie–Weiss (CW) fit to the data from 100 to 300 K. The high-temperature CW fit yields an effective magnetic moment $\mu_{\text{eff}}=3.98\mu_B$/f.u. and a CW temperature $\Theta_{\text{CW}}=4.1$ K. The calculated value of μ_{eff} is enhanced over the Pr^{3+} free ion value of $3.58\mu_B$/f.u., which is possibly due to a contribution from the $[Fe_4As_{12}]$ sublattice. If the Pr^{3+} and $[Fe_4As_{12}]$ contributions to the magnetic susceptibility can each be described by CW laws with the same value of Θ_{CW}, then $\mu_{\text{eff}}^{[Fe_4As_{12}]}$ can be estimated from

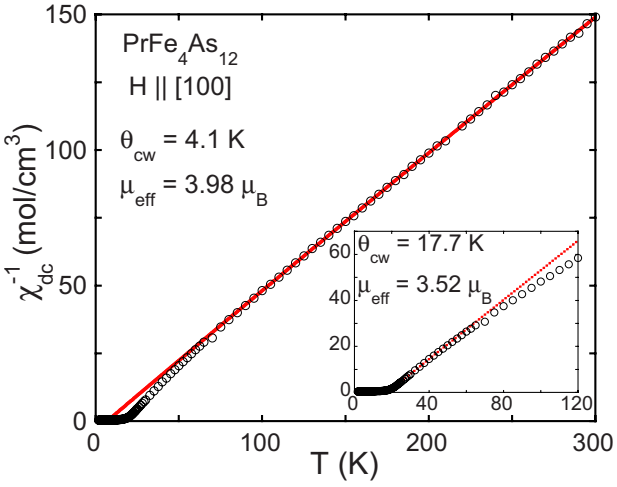

FIG. 1. (Color online) Inverse dc magnetic susceptibility χ_{dc}^{-1} vs temperature T data for $PrFe_4As_{12}$ from 1.8 to 300 K in a 0.5 T magnetic field that is applied along the [100] crystallographic direction. Curie–Weiss fits from 70 to 300 K (solid line in the main panel) and from 20 to 40 K (dashed line in the inset) result in quantities as displayed.

$$\mu_{\text{eff}}^{\text{meas}}=\sqrt{(\mu_{\text{eff}}^{\text{Pr}})^2+(\mu_{\text{eff}}^{[Fe_4As_{12}]})^2}, \tag{1}$$

where $\mu_{\text{eff}}^{\text{meas}}=3.98\mu_B$/f.u. and $\mu_{\text{eff}}^{\text{Pr}}=3.58\mu_B$/f.u., which are the value that is found from the CW fit and the theoretical Pr^{3+} free ion moment, respectively. Equation (1) yields $\mu_{\text{eff}}^{[Fe_4As_{12}]}=1.74\mu_B$/f.u. This value falls between several isomorphic compounds. In $PrFe_4P_{12}$, there is no sign of a moment on the $[Fe_4P_{12}]$ sublattice with $\mu_{\text{eff}}=3.62\mu_B$/f.u. being very close to the Pr^{3+} free ion value;[8] this value is lower than $\sim2.7\mu_B$/f.u. that is found for the $[Fe_4Sb_{12}]$ sublattice moment in $PrFe_4Sb_{12}$.[24–26] Furthermore, for $FeSb_3$, i.e., the unfilled skutterudite parent compound, Danebrock *et al.*[26] proposed that each iron atom would be expected to have a d^5 configuration with a single unpaired electron per iron atom. They went on to suggest that the transfer of three electrons from the La^{3+} ion in the filled skutterudite $LaFe_4Sb_{12}$ would leave only a single Fe ion per f.u. with an uncompensated electron in a magnetic d^5 configuration. From $\mu_{\text{eff}}=2[s(s+1)]^{1/2}\mu_B$, a value of $\mu_{\text{eff}}=1.73\mu_B$ would be expected for the spin-only value of a Fe^{3+} ion with the low spin d^5 state.[26] The values that were found by Danebrock *et al.*[26] for the Fe ions in $LaFe_4Sb_{12}$, i.e., $\mu_{\text{eff}}=3.0\mu_B$/f.u., were higher than this prediction. It can be argued that this discrepancy is due to incomplete filling of the La sites, which results in a larger

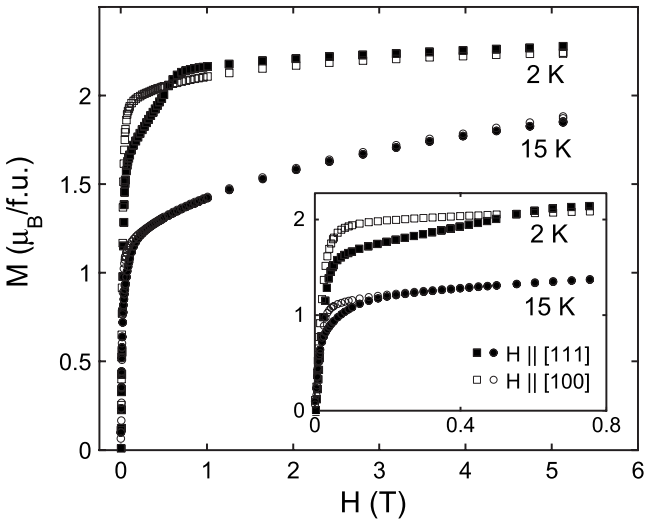

FIG. 2. Magnetization M vs magnetic field H for 2 K (squares) and 15 K (circles) isotherms in fields that are applied along the [111] (solid symbols) and [100] (open symbols) crystallographic directions. The 2 K isotherms show a change in the easy axis at $H=0.8$ T from the [100] to the [111] directions. This change is not observed in the 15 K data, which indicates that the easy axis does not change at higher temperatures.

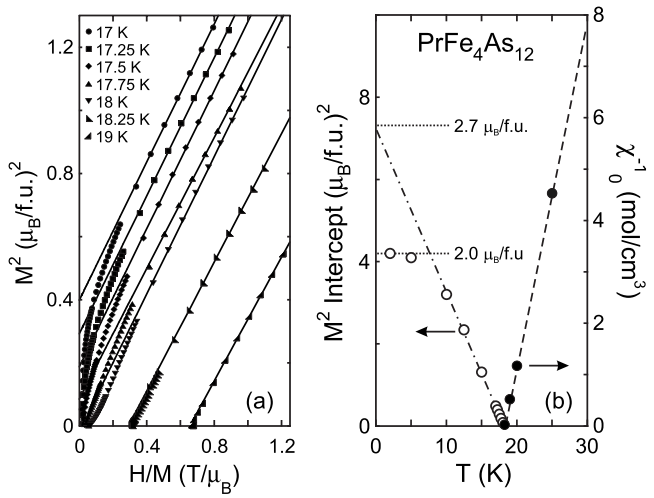

FIG. 3. (a) Arrott plots of M^2 vs H/M isotherms for $PrFe_4As_{12}$ between 17 and 19 K. The solid lines are linear fits to the isotherms and are used to extrapolate $\chi_0^{-1}=H/M$ to $M=0$ and M to $H=0$. (b) Temperature dependence of the M^2 intercepts (open circles) from the Arrott plots in (a) are shown with linear extrapolation (dashed-dotted line) of the data above 10 K that are used to estimate $M(0)=2.7\mu_B$/f.u. Temperature dependence of the inverse susceptibility (solid circles) is also shown with a linear Curie–Weiss fit (dashed line) of the data from 18 to 25 K.

fraction of Fe ions with uncompensated spins. Interestingly, if a similar electron transfer argument is made for $PrFe_4As_{12}$, the $\mu_{\text{eff}}=1.74\mu_B$/f.u. of $[Fe_4As_{12}]$ is well described by the model.[27]

Since the slight curvature in $\chi_{\text{dc}}^{-1}(T)$ below 75 K may be due to CEF effects, a low-T, i.e., 19.5–45 K, CW fit was also performed (see the inset of Fig. 1) to estimate the CEF split ground state moment. (Although the Pr^{3+} ion is in a tetrahedral T_h CEF environment, cubic O_h symmetry provides a close approximation for $PrFe_4As_{12}$ in low fields and, due to its relative simplicity, was employed to analyze the CEF effects.) A cubic CEF splits the Pr^{3+} ninefold degenerate $J=4$ Hund's rule ground state multiplet into a nonmagnetic Γ_1 singlet, a nonmagnetic Γ_3 doublet, and magnetic Γ_4 and Γ_5 triplets. The low-T CW fit yields the values $\mu_{\text{eff}}=3.52\mu_B$/f.u. and $\Theta_{\text{CW}}=17.7$ K. By utilizing Eq. (1) with $\mu_{\text{eff}}^{\text{meas}}=3.52\mu_B$/f.u. and $\mu_{\text{eff}}^{[Fe_4As_{12}]}=1.74\mu_B$/f.u., which is from the high-temperature analysis, the effective moment for the CEF split Pr^{3+} $J=4$ multiplet is found to be $3.06\mu_B$/f.u. The large value of the low-temperature effective moment implies contributions from multiple Pr^{3+} CEF energy levels, which indicates a minimal CEF splitting prior to the onset of magnetic ordering.

Figure 2 shows the magnetization vs field, $M(H)$, isotherms of $PrFe_4As_{12}$ at 2 and 15 K. The magnetic field H was swept from 0 to 5.5 T while oriented along both the [100] and the [111] crystallographic directions. A shift in the maximal value of the 2 K $M(H)$ isotherm, which is from $H\|[100]$ to $H\|[111]$, occurs above 0.8 T. This change in maxima likely indicates a change in the magnetic easy axis, which is from the [100] to the [111] direction, as the field is increased at this temperature. No shift in magnitude was detected in the 15 K isotherm, which suggests that the magnetic easy axis remains along the [100] direction for temperatures between Θ_C and T_{irr} [as seen in Fig. 5(a)]. A similar low field $M(H)$ behavior is observed in UFe_4P_{12} below T_{irr} [the relative maxima, of the $M(H)$ isotherms, between the [110] and the [111] directions change as the field is increased].[28] However, in UFe_4P_{12}, T_{irr} and Θ_C coincide at 3 K and the magnetic easy axis remains *unchanged* along the [100] direction.

Additionally, from the 2 K $M(H)$ isotherm of $PrFe_4As_{12}$, a saturating magnetization M_s of $2.3\mu_B$/f.u. by 5.5 T was observed (consistent with a magnetic Γ_5 triplet ground state, wherein $M_s=2.0\mu_B$/f.u. is expected). Furthermore, additional low-temperature $M(H)$ hysteresis sweeps (not shown) reveal a coercive field of $H_c=1.1$ mT and a remnant magnetization $M_{\text{rem}}=0.43\mu_B$/f.u.

At temperatures around Θ_{CW}, $M(H)$ measurements with $H\|[100]$ (plotted as M^2 vs H/M in Fig. 3) indicate the development of a spontaneous moment. An Arrott analysis yields a Curie temperature Θ_C of 18.2 K—which is close to the value of Θ_{CW}. Figure 3(b) shows the M^2 intercepts of the Arrott plots vs T. A linear extrapolation of the M^2 intercepts around the critical temperature yields a magnetization at zero temperature $M(0)=2.7\mu_B$/f.u., whereas the actual M^2 intercept vs T data reveal a spontaneous magnetization M_s at the zero temperature of $2.0\mu_B$/f.u., which is comparable to M_{sat} (at 5.5 T). The inverse initial susceptibilities χ_0^{-1}, which are derived from the Arrott plots, are displayed (on the right axis) in Fig. 3(b) as a function of temperature along with a CW fit. Values for the effective moment and Θ_{CW} that are obtained from the fit are consistent with those derived from the low-T CW fit of the $\chi_{\text{dc}}^{-1}(T)$ data.

The real and imaginary parts of the ac magnetic susceptibility vs temperature, $\chi'_{\text{ac}}(T)$ and $\chi''_{\text{ac}}(T)$, of $PrFe_4As_{12}$ are plotted as functions of temperature in Fig. 4. The midpoint of the increases in both $\chi'_{\text{ac}}(T)$ and $\chi''_{\text{ac}}(T)$ indicates the onset of

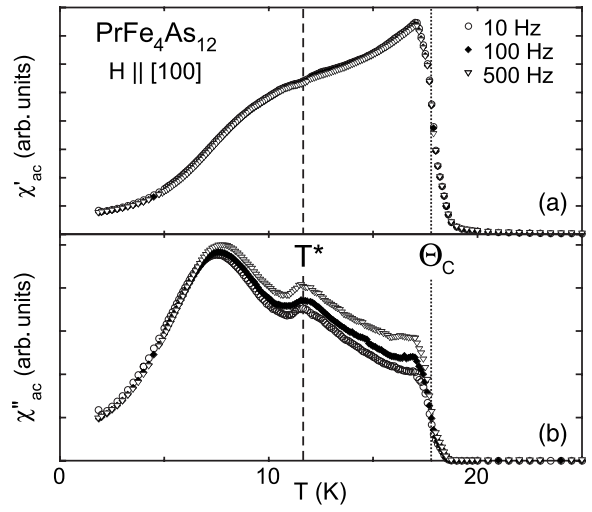

FIG. 4. Temperature T dependence of the real χ'_{ac} and imaginary χ''_{ac} parts of the ac magnetic susceptibility of $PrFe_4As_{12}$ for three driving frequencies of 10, 100, and 500 Hz with a driving field of 0.1 mT that is applied along the [100] direction.

magnetic order below 17.8 K, which is close to the value of Θ_C that is obtained from the Arrott analysis. A very slight kink is observed in $\chi'_{ac}(T)$ at $T \sim 12$ K, as well as a shoulder near 10 K; additionally, there is a change in curvature at $T \sim 7.5$ K. The first feature, which is near 12 K, is associated with a peak in $\chi''_{ac}(T)$ at 11.7 K, while the inflection point at 7.5 K corresponds to a second peak seen in $\chi''_{ac}(T)$. The shoulder in $\chi'_{ac}(T)$ seems tied to the trough between the two peaks observed in $\chi''_{ac}(T)$. Only a slight change in amplitude of $\chi'_{ac}(T)$ is detected as the drive frequency is increased. However, a clear increase in the magnitude of $\chi''_{ac}(T)$ is found for temperatures between 6.8 K and Θ_C with increasing drive frequency; the transition at Θ_C and the peak at 12.5 K do not appear to shift in temperature with frequency, while a very slight shift, which is on the order of 0.3 K, is observed for the peak at 7.5 K as the frequency is raised from 10 to 500 Hz. A comparable behavior in $\chi_{ac}(T)$ was observed in $RFe_{10}Mo_2$ (R=rare earth) compounds.[29] In these systems, the sharp transition in $\chi'_{ac}(T)$ is due to the onset of magnetic ordering, and the broad, shoulderlike features are attributed to spin reorientations.

The behavior of the magnetization as a function of temperature, $M(T)$, in the ordered state is displayed in Fig. 5(a) for $1.8 \leq T \leq 30$ K and 5 mT $\leq H \leq 5$ T, with the fields oriented along the [100] crystallographic direction. For the 5 mT field-cooled and zero-field-cooled data, a spontaneous moment develops below 17.8 K [seen as the minimum in $dM(T)/dT$ that is plotted in Fig. 5(b)]. A weak irreversibility is observed at 16.9 K, while a significant irreversibility (as well as a maximum in the zero-field-cooled data) occurs at T_{irr}=11.5 K. The irreversibility is suppressed with field and vanishes by 50 mT, which results in a continuous increase in $M(T)$ below Θ_C for $H \| [100]$. The irreversibility that develops in the $M(T)$ data is consistent with both spin glass behavior and narrow Bloch walls.[30,31] However, the small coercive field of 1.1 mT and the remnant magnetization of $0.43 \mu_B$/f.u. are not typical of systems with narrow Bloch

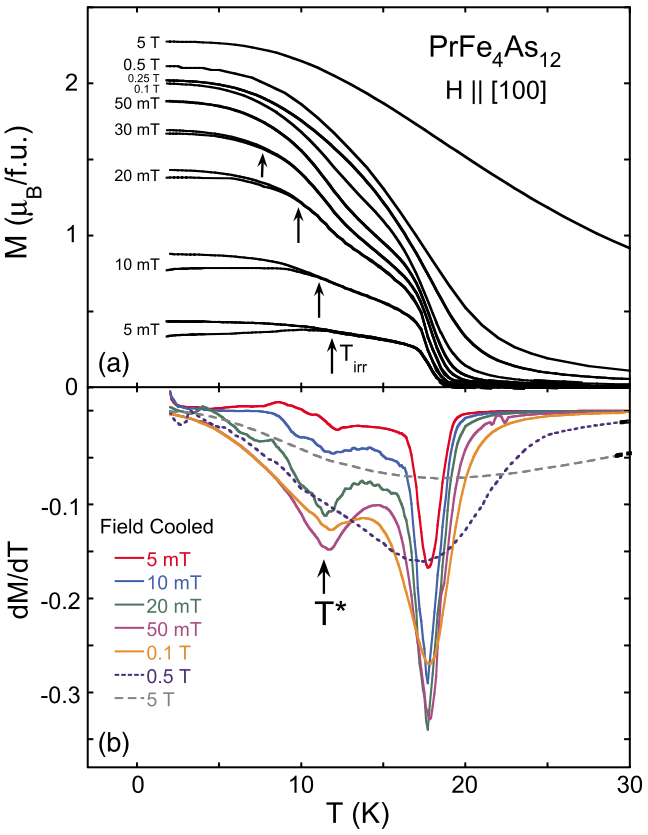

FIG. 5. (Color online) (a) Zero-field-cooled and field-cooled magnetization data for $PrFe_4As_{12}$ for constant magnetic fields between 5 and 5 T that are applied along the [100] crystallographic direction. (b) Temperature derivatives of the field-cooled magnetization. Local minima in dM/dT are identified with characteristic temperatures T^* and Θ_C in the low-field limit.

walls;[32–34] yet, neither the cusp nor the typical frequency dependence of a spin glass is found in the ac susceptibility (Fig. 4). As can be seen in Fig. 5(b), the minimum of $dM(T)/dT$ at 17.8 K does not appreciably shift with field from 5 mT to at least 0.5 T. An additional minimum at $T^* \simeq 12$ K is observed in $dM(T)/dT$, and it also does not shift with increasing field but vanishes for $H > 0.5$ T.

B. Specific heat

The specific heat vs temperature, $C(T)$, of $PrFe_4As_{12}$ is presented in Fig. 6, revealing a sharp, discontinuous feature at Θ_C=18 K, a shoulder near 10 K, and an upturn below $T \sim 2$ K due to a nuclear Schottky anomaly. The specific heat C is composed of magnetic C_m, conduction electron C_e, nuclear C_n, and phonon C_l contributions (i.e., $C = C_m + C_e + C_n + C_l$). In order to analyze the behavior of C_m and C_e in the ordered state, it is necessary to remove C_l and C_n. To estimate C_l of $PrFe_4As_{12}$, two separate analytic methods were used since the specific heat of a suitable nonmagnetic analog of $PrFe_4As_{12}$ (e.g., $LaFe_4As_{12}$) has not been reported yet. Fits of the data to $C/T = \gamma + \beta T^2$ for temperatures above Θ_C yield an electronic contribution γ=390 mJ/mol K^2 and a Debye temperature θ_D=356 K that are calculated from the fit value of β. However, since the T^3 behavior of the lattice

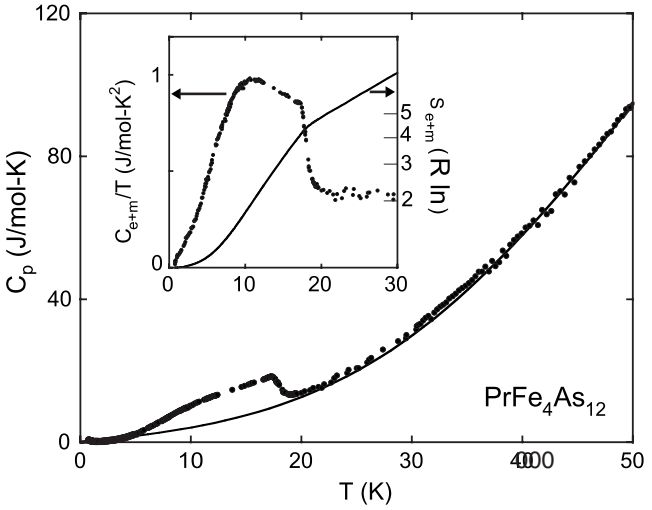

FIG. 6. Temperature dependence of the total specific heat of $PrFe_4As_{12}$, with Debye function fit (solid line) of Eq. (2) plus a constant electronic term. Inset: electronic plus magnetic portions of the specific heat that are obtained from subtracting lattice and nuclear contributions [see text (circles)]. The solid line is the associated entropy s_{e+m}.

specific heat is strictly valid only for the lowest temperatures, $T \leq \theta_D/50$, the specific heat data above the transition were also modeled by using a second method, i.e., a Debye function,

$$C_l(T) = \frac{9rRT^3}{\theta_D^3}\int_0^{\theta/T}\frac{x^4e^x}{(e^x-1)^2}dx, \qquad (2)$$

along with a linear electronic term. This method results in a better fit to the data, yielding the same $\theta_D = 356$ K and a slightly smaller $\gamma = 340$ mJ/mol K^2. The value of θ_D is consistent with the decreasing Debye temperatures of $PrRu_4As_{12}$ ($\theta_D = 344$ K) and $PrOs_4As_{12}$ ($\theta_D = 260$ K) [19,20] as the lattice size increases with increasing ionic radius of the relevant transition metal. The values of γ that are obtained for $PrFe_4As_{12}$ also fall between those of $PrRu_4As_{12}$ ($\gamma = 73$ mJ/mol K^2) [16] and of $PrOs_4As_{12}$, which has $\gamma \approx 1$ J/mol K^2 in its antiferromagnetically ordered state below 1.6 K (for $PrOs_4As_{12}$, $\gamma \approx 50-200$ mJ/mol K^2 for $10 \leq T \leq 18$ K, depending on the applied magnetic field).[19,20] [It should be noted that θ_D depends on the temperature range over which the fit is performed; for this reason, further measurements of $C(T)$ at higher temperatures and of appropriate analog materials will be necessary to better determine the lattice contribution and, subsequently, the value of γ.]

To analyze the nuclear contribution to the specific heat C_n, the upturn in $C(T)$ below 2 K was modeled by an $\sim 1/T^2$ dependence of the high-temperature side of a Schottky contribution.[35] At the lowest temperatures, at which C_n dominates, a fit of $CT^2 = a + bT^{2+n}$ was performed by using the power law term to model the combined low-temperature magnetic and electronic portions of the specific heat. This fit results in $a = 360$ mJ K/mol, and from this, a magnetic interaction parameter, $a' = \sqrt{3a/\{R[I(I+1)]\}}$, can be calculated. [The small quadrupole term of Pr (~ 0.08 b) has a little effect on the calculations at these relatively high temperatures, and so was not used for the analysis.] For $PrFe_4As_{12}$, the value of $a' = 0.12$ K that is obtained falls between the experimental (0.0624 K) and theoretical (0.210 K) values for Pr.[36] Note that the As ion has a nuclear magnetic moment of the same order ($1.44\mu_N$ compared to $4.28\mu_N$ of Pr)[37] as well as a larger quadrupole term (0.316 vs −0.077 b for Pr);[37] therefore, future work in fields (and at lower temperatures) could help to determine the relative contributions of the Pr and As ions, in addition to distinguishing the effects due to the nuclear dipole and quadrupole moments.

The inset of Fig. 6 presents a plot of the electronic plus magnetic contributions to the specific heat, $C_{e+m} \equiv C - C_n - C_l$, vs temperature T, which is obtained by subtracting the lattice and nuclear portions of the specific heat. As previously mentioned, a sharp increase in $C_{e+m}(T)$ at 18 K is consistent with Θ_C that is found in $M(T,H)$, χ_{ac}, and Arrott plot analysis, which is discussed in the prior section. This clear feature in $C(T)$ and other properties at the Curie temperature of $PrFe_4As_{12}$ is in marked contrast to the broad transition that is observed in its sister compound, $PrFe_4Sb_{12}$,[25] which may be complicated by an underlying Schottky anomaly. With decreasing temperature, $C_{e+m}(T)/T$ goes through a peak near 10 K before falling *below* the value of γ that is obtained from fits in the paramagnetic region. In fact, $C_{e+m}(T)/T$ appears to approach zero as $T \to 0$—which is an indication of a possible gap opening in the Fermi surface at some temperature below Θ_C. While this is not expected in relation to simple ferromagnetic order, a gapped behavior arising from a possible change in magnetic and/or structural character below Θ_C may explain this observation.

The inset of Fig. 6 (right axis) also displays the combined electronic and magnetic portions of the entropy vs temperature, $S_{e+m}(T)$, of $PrFe_4As_{12}$; at the maximum in $C(T)/T$, the entropy released has reached R ln 2, while at Θ_C, the entropy released is near R ln 4. Because of the difficulty in separating the magnetic and electronic contributions of the specific heat below the ferromagnetic transition, the implications of the values of released entropy remain to be determined. However, by using an equal entropy argument at Θ_C, the entropy released due to the electronic portion must be near R ln 2.3 at the transition. This leaves an entropy of R ln 2 released due to the magnetic portion, implying a spin degeneracy of 2, although the only doublet ground state available to $PrFe_4As_{12}$ is the Γ_3 state, which is nonmagnetic. Moreover, $M(T,H)$ measurements indicate a Γ_5 triplet state as the most likely ground state. These facts seem to indicate a case wherein a portion of the magnetic entropy is transferred to the conduction electrons.

The overall behavior of $C(T)/T$ for $PrFe_4As_{12}$ is similar to those of other ferromagnetic skutterudites. In particular, the broad maximum below the Curie temperature is quite similar to the behavior in EuT_4Sb_{12} (T=Fe, Ru, and Os), which was explained by using a mean-field analysis.[38] However, for $PrFe_4As_{12}$, these features cannot be simply explained by using a mean-field analysis. The shoulder observed in $C_m(T)/T$ of mean-field systems develops when the total angular momentum $J \geq 2$,[39] while for $PrFe_4As_{12}$, a $J=1$ triplet state is consistent with a Γ_5 ground state that is inferred from M_{sat}. However, by combining the contribution C_m from such a

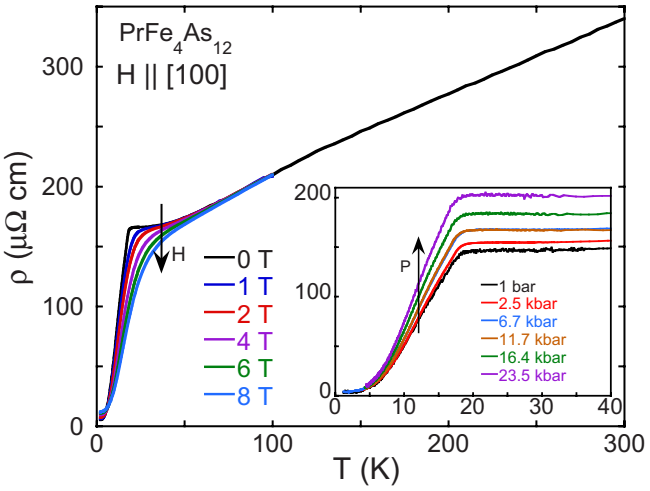

FIG. 7. (Color online) Temperature dependence of electrical resistivity ρ for $PrFe_4As_{12}$ for magnetic fields of up to 8 T that are applied along the [100] direction. Inset: (zero-field) temperature dependence of resistivity under applied pressures from 1 to 23.5 kbar. (Note that the values for 6.7 and 11.7 kbar overlap and are difficult to distinguish.)

mean-field transition with a Schottky contribution C_s due to a low-lying excited state and a constant electronic contribution C_e, the overall behavior below the transition can be modeled very well [excluding the lowest temperatures, $T \leq 6$ K, at which $C_{e+m}(T)/T \rightarrow 0$]. Other (nonskutterudite) systems are seen to have a similar behavior, which include UGe_2 (Ref. 40) and β-UB_2C.[40–42] Attempts to explain the shoulders in $C_m(T)/T$ of these systems include a coupled charge-density wave and spin-density wave transition. In addition, the similar behavior of $C(T)$ and $\chi'_{ac}(T)$ [Fig. 4(a)] as well as $C(T)/T$ and $d\rho(T)/dT$ (see Fig. 12) for temperatures below the Curie temperature suggests an underlying phenomenon in $PrFe_4As_{12}$ that strongly couples to all of these quantities, as a change in the nature of the ordering would.

C. Transport and thermopower

1. Electrical resistivity

The electrical resistivity ρ of $PrFe_4As_{12}$ is presented in Fig. 7 as a function of temperature T in the temperature range of 1.9–300 K for various applied fields ($H \| [100]$) up to 8 T. The electrical resistivity $\rho(T)$ of $PrFe_4As_{12}$ decreases with temperature from 300 $\mu\Omega$ cm at 300 K, which exhibits a metallic behavior that is very similar to that of its Os-based counterpart $PrOs_4As_{12}$. In $PrFe_4As_{12}$, however, $\rho(T)$ sharply drops below $\Theta_C = 18$ K, which indicates a dramatic decrease in scattering below the onset of long range magnetic order. Several fitting methods were used to characterize $\rho(T)$ in the ordered state below Θ_C, which include (1) a gapped function that characterizes electron-spin wave scattering [as was done for both ferromagnetic systems EuB_6 (Ref. 43) and $NdOs_4Sb_{12}$ (Ref. 44)], which gives a gap magnitude of $\Delta = 11.0$ K for $PrFe_4As_{12}$, and (2) a simple power law fit (i.e., $\rho = \rho_0 + aT^n$), which gives $\rho_0 = 4.3$ $\mu\Omega$ cm, $n = 2.9$, and $a = 0.069$ $\mu\Omega$ cm/K^n, with both methods yielding comparably good fits below 12 K.

Fixing the power law to a quadratic [i.e., $\rho(T) = \rho_0 + AT^2$] results in a scattering coefficient $A = 0.56$ $\mu\Omega$ cm/K^2, which, when compared to the electronic specific heat coefficient $\gamma = 340$ mJ/mol K^2, gives a value of 4.8 $\mu\Omega$ cm mol^2 K^2/J^2 for the Kadowaki–Woods ratio A/γ^2, which is reasonably close to the universal value[45] of 10 $\mu\Omega$ cm mol^2 K^2/J^2. This suggests that the value of γ that is extracted from specific heat analysis is reasonable and that electron-electron scattering is the dominant scattering mechanism at low temperatures. However, as will be discussed in Sec. IV, the similarity of the temperature derivative of the electrical resistivity, $d\rho(T)/dT$, to the electronic and magnetic portions of specific heat $C(T)/T$ over almost the entire temperature range below Θ_C (see Fig. 12) indicates that the temperature dependence of the resistivity is more simply dictated by the spin entropy (i.e., disorder), and it is thus more instructive to directly consider the form of specific heat, as discussed above.[47]

At the lowest temperatures, $\rho(T)$ eventually decreases toward a saturating residual value $\rho_0 = 4.3$ $\mu\Omega$ cm, which corresponds to a very large zero-field residual resistivity ratio $\rho(300\ \text{K})/\rho_0 \simeq 75$ that is comparable to that observed in $PrOs_4As_{12}$,[19] reflecting the high quality of both single-crystal growths. As a function of magnetic field, an increasing negative magnetoresistance (MR) is found between ~6 and ~60 K, with an increasing rounding of the shoulder in $\rho(T)$ at Θ_C, as shown in Fig. 7. The overall decrease in ρ with increasing field around the magnetic transition is qualitatively consistent with an expected decrease in spin disorder scattering with increasing field-induced polarization of the unordered spins. Moreover, the apparent broadening of the transition—which is also seen in magnetization around Θ_C, as shown in Fig. 5—is also consistent with this picture and is also similar to that observed in EuB_6.[43] Yet, at lower temperatures, a slight positive magnetoresistance is observed below ~6 K, which indicates a gradual increase in the residual resistivity with a field consistent with a standard metallic behavior deep in the ordered state, wherein spin disorder scattering is negligible. Indeed, the MR in the zero-temperature limit [i.e., $\rho_0(H)$] is approximately linear in a field of up to at least 5 T, with signs of saturation at higher fields (not shown) similar to the behavior observed for $NdOs_4Sb_{12}$.[44]

The inset of Fig. 7 displays the (zero-field) pressure dependence of $\rho(T)$ from 1.1 to 40 K for applied pressures of up to 23.5 kbar. As shown, Θ_C remains approximately constant with pressure in this range along with ρ_0, while the magnitude of $\rho(T)$ just above Θ_C linearly increases with pressure at a rate of ~2.3 $\mu\Omega$ cm/kbar. This is to be compared and contrasted to the negligible pressure dependence of $\rho(T)$ in $PrOs_4As_{12}$,[19] which suggests subtle differences in the responses of electronic scattering between these two systems to changes in the lattice density.[48]

2. Thermal conductivity

The thermal conductivity κ vs temperature T of $PrFe_4As_{12}$ was measured down to 2 K in zero and applied fields that are directed along the [100] crystallographic axis, as shown in the main panel of Fig. 8. Above ~20 K, $\kappa(T)$ is dominated

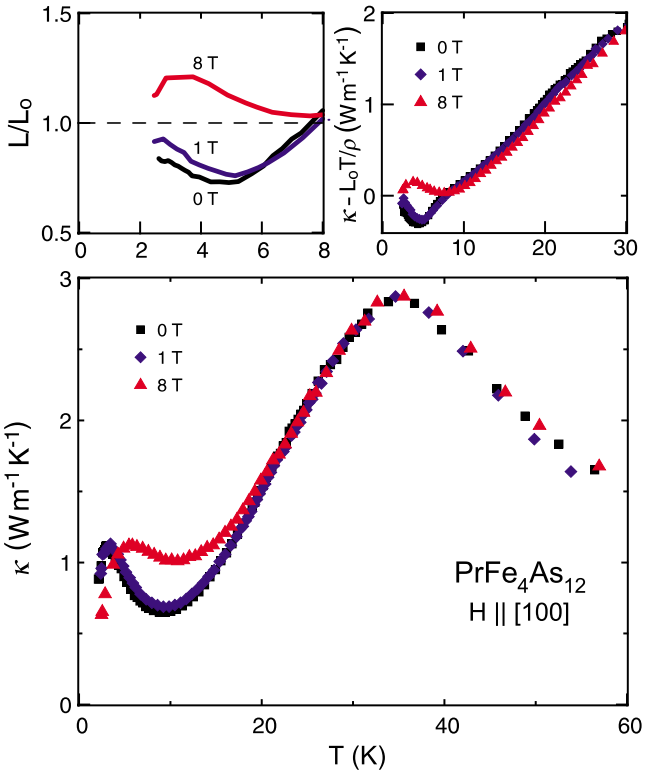

FIG. 8. (Color online) Thermal conductivity of $PrFe_4As_{12}$ in zero and applied fields with $H\|[100]$. The top-left panel presents the ratio of heat and charge conductivities, which is plotted as the Lorenz number $L=\frac{\kappa\rho}{T}$ normalized to the WF law expectation $L_0=2.44\times10^{-8}$ Ω W/K^2. The top-right panel plots the thermal conductivity remaining after subtraction of the electronic contribution estimated using the WF law (see text).

by the lattice contribution to the total thermal conduction. This is evidenced by a lack of field dependence on $\kappa(T)$ above this temperature, which is in contrast to that of $\rho(T)$, which shows a magnetoresistance of up to ~60 K. As expected for phonon heat conduction, a maximum in $\kappa(T)$ near ~35 K marks the crossover between dominant phonon scattering mechanisms: as the temperature is lowered, the probability of umklapp-dominated scattering processes exponentially decreases and the phonon mean free path rises until sample boundaries limit any further increase. Empirically, this maximum usually occurs near $\sim\Theta_D/10$ in single-crystal specimens.[49] As shown in Fig. 8, a maximum in $\kappa(T)$ near ~35 K corresponds well to $\theta_D=356$ K, which is obtained from the specific heat analysis that is previously discussed.

At lower temperatures, the electronic contribution to $\kappa(T)$ becomes significant due to the dramatic increase in charge conductivity below T_c, which results in a notable field dependence that mimics that of $\rho(T)$. Below ~10 K, the electronic contribution to $\kappa(T)$ becomes dominant, as evidenced by the observation of the Wiedemann–Franz (WF) law around 8 K, at which the ratio of heat to charge conductivities—which is known as the Lorenz number and given by $L=\frac{\kappa\rho}{T}$—becomes equal to the Sommerfeld value $L_0=2.44\times10^{-8}$ Ω W/K^2 (Fig. 8, top left panel). At still lower temperatures, a further decrease in L at 0 and 1 T—which is most likely due to inelastic scattering of electronic heat carriers (see, e.g., Ref. 49)—eventually turns over toward a recovery of the WF law expectation at $T=0$ K.

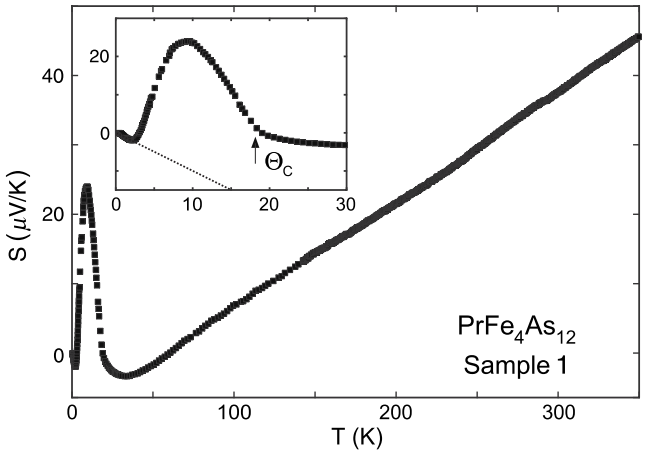

FIG. 9. Thermoelectric power of $PrFe_4As_{12}$ with heat currents directed along the principal [100] axis. The inset shows the low-temperature behavior, which highlights the coincidence of the ferromagnetic transition Θ_C and a kink in $S(T)$. The dotted line is a linear extrapolation of data below 2 K.

At high fields, there appears to be an *additional* contribution to heat conductivity, as evidenced by an enhanced Lorenz number below 8 K in the 8 T data that are shown in the top-right panel of Fig. 8. Because plotting $L(T)$ in effect normalizes out any change in electronic (heat and charge) conduction due to magnetoresistance and because phonon conduction is not expected to change with field, this increase points to an additional thermal excitation. A subtraction of the electronic component L_0T/ρ (estimated by using the WF law) from the total thermal conductivity is a method commonly used to give an approximate measure of the total remaining heat conduction due to other sources, such as phonons and magnons. As shown in the top-right panel of Fig. 8, there is a dominant contribution above 10 K, which is roughly independent of field as expected for phonon carriers. Below 10 K, the 8 T data indeed show an enhanced value with a peak near ~4 K (apparent negative values at 0 and 1 T are due to inelastic scattering). While this additional contribution is possibly associated with the appearance of magnon excitations deep in the ordered state, it is not clear why magnon conduction would be enhanced with field and, moreover, why it would not remain negligible compared to the electronic contribution as it is at lower fields and as typically found in other metallic magnets.[50] Because the onset of this additional contribution appears below 10 K, the temperature at which several other features appear in measured quantities (see Sec. IV), other possible scenarios cannot be ruled out. For instance, a change in the ordering structure with field would introduce a change in the magnon spectrum.

3. Thermopower

The thermoelectric power vs temperature, $S(T)$, of $PrFe_4As_{12}$ was measured between 0.5 and 350 K, with heat currents that are directed along the principal [100] axis, as shown in Fig. 9. Starting at a modestly large value of

$\sim 33\ \mu V/K$ at room temperature, the Seebeck coefficient $S(T)$ continuously falls with temperature, crossing zero near 70 K and continuing to decrease toward Θ_C, at which it undergoes an abrupt increase toward a maximum at lower temperatures before returning toward zero value, as expected at $T=0$ K. The striking linearity of $S(T)$ from ~ 40 K to above 350 K is typical of low-carrier density metals and has indeed been observed in similar materials, such as $YbFe_4Sb_{12}$.[53] As done for the latter compound, the slope of $S(T)$ in this region can be attributed to electron thermal diffusion and used to extract a value for the Fermi energy of $E_F \simeq 0.52$ eV (or 6000 K).

As shown in the inset of Fig. 9, the onset of magnetic order at Θ_C appears to coincide with a kink in $S(T)$, which provides another measure of the ordering temperature as well as additional insight into the change in scattering behavior at the transition: an abrupt *increase* in the thermopower coincides with the dramatic drop in scattering, as exhibited by $\rho(T)$. Below 3 K, $S(T)$ again crosses zero to reach a small negative value before returning toward zero at $T=0$ K in an approximately linear manner, with a limiting slope of $\lim_{T\to 0} S/T \simeq -1\ \mu V/K^2$, as shown in the inset of Fig. 9. A recent investigation of thermoelectric power in correlated materials has highlighted an interesting relation between the Seebeck coefficient and the electronic specific heat,[51] which shows the universal ratio $q=\frac{S}{T}\frac{N_A e}{\gamma}$ between the electronic specific heat coefficient γ and the limiting value of S/T remains close to $q=\pm 1$, which is both in a simple theoretical picture and empirically for a wide range of correlated materials. In $PrFe_4As_{12}$, the zero-field value of $q \simeq -0.3$ also follows this relation rather well and is comparable to the value of $q(5.5\ T)=+0.6$ found in the field-induced normal state of the strongly correlated skutterudite $PrFe_4P_{12}$.[52] A single-band, single-scatterer picture is most likely inadequate for correctly explaining correlation effects in $PrFe_4As_{12}$, as is surely the case for the (zero-field) antiferroquadrupolar-ordered state in $PrFe_4P_{12}$, which indeed results in a large value of $q(0\ T) \simeq -60$.[52] However, it is perhaps not surprising that the field-induced normal (paramagnetic) state in the latter is comparable to that of $PrFe_4As_{12}$, given the expectation of similar electronics and carrier concentrations in both materials.

As a function of field, the thermopower exhibits an interesting shift in behavior below Θ_C, as shown in Fig. 10(a). With increasing field, both the peak in $S(T)$ (below Θ_C) and the kink associated with Θ_C itself shift in parallel up to higher temperatures, which increase by approximately $\sim 6-7$ K at 8 T to ~ 15 and ~ 25 K, respectively. The latter can be more precisely defined by identifying the transition with a peak in $d^2S(T)/dT^2$ (not shown), which gives an increase of Θ_C to ~ 19.5 K at 1 T and ~ 25 K at 8 T. Interestingly, this increase is much more dramatic than the inflection point in magnetization, as shown in Fig. 5, which shows a negligible increase up to 5 T.

The thermoelectric figure of merit $ZT=S^2T/(\rho\kappa)$ for $PrFe_4As_{12}$ was calculated by using resistivity, thermal conductivity, and thermopower data that are taken in various fields for the same sample. As was the case for $YbFe_4Sb_{12}$,[53] the value of ZT in $PrFe_4As_{12}$ is small ($\ll 1$) at high temperatures. As shown in Fig. 10(b), ZT reaches quite small values

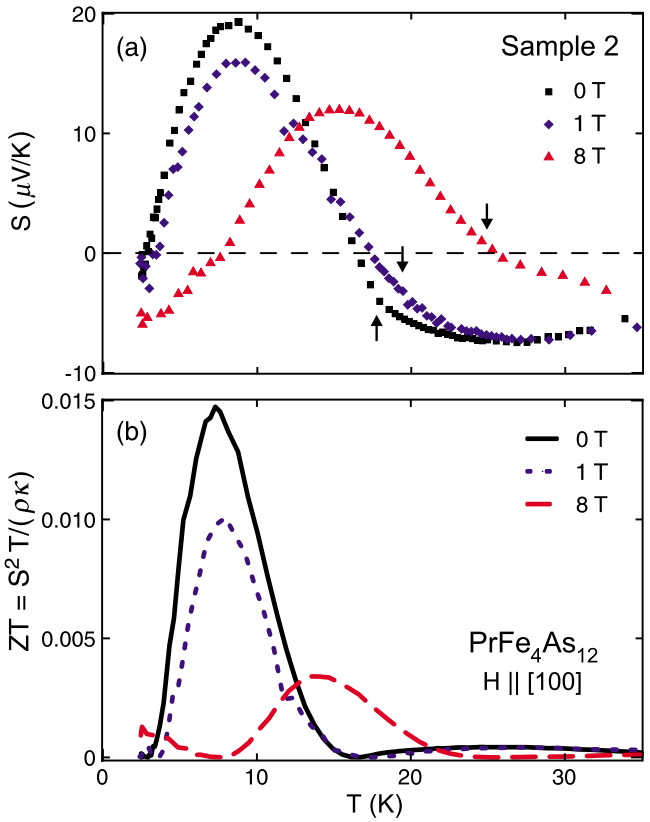

FIG. 10. (Color online) (a) Thermoelectric power of $PrFe_4As_{12}$ taken in various fields ($H\|[100]$), with the arrows indicating the position of the kink in $S(T)$ associated with Θ_C (see text). (b) Dimensionless thermoelectric figure of merit ZT that is obtained from the data in (a) (see text).

at lower temperatures before rising to a peak value of ~ 0.015 near 12 K in the zero-field, ordered state. As a function of magnetic field, this peak is seen to be substantially suppressed, which decreases to ~ 0.004 at 8 T. The temperature dependence of ZT thus appears to mimic that of $S(T)$, including both the shift in peak position and the decrease in magnitude with increasing field.

D. Ultrasound

Ultrasonic measurements were performed in order to investigate a quadrupole contribution for the successive transitions of $PrFe_4As_{12}$. Relative changes in the elastic constants $\Delta C_{44}(T)/C_{44}$ and $\Delta C_{11}(T)/C_{11}$ of a $PrFe_4As_{12}$ single crystal are shown in Fig. 11. The transverse C_{44} mode corresponds to the strains ε_{yz}, ε_{zx}, and ε_{xy} associated with Γ_5 symmetry, while the longitudinal C_{11} mode corresponds to the strain

$$\varepsilon_{zz} = \frac{\varepsilon_{xx}+\varepsilon_{yy}+\varepsilon_{zz}}{3} + \frac{2\varepsilon_{zz}-\varepsilon_{xx}-\varepsilon_{yy}}{3}, \qquad (3)$$

associated with Γ_1 and Γ_{23} symmetry strains.[46] In the temperature region from 200 to 50 K, both elastic constants show a monotonic increase. The transverse C_{44} mode exhibits a small softening of 0.2% down to 18 K with a broad maximum around 50 K, which may be due to a weak CEF

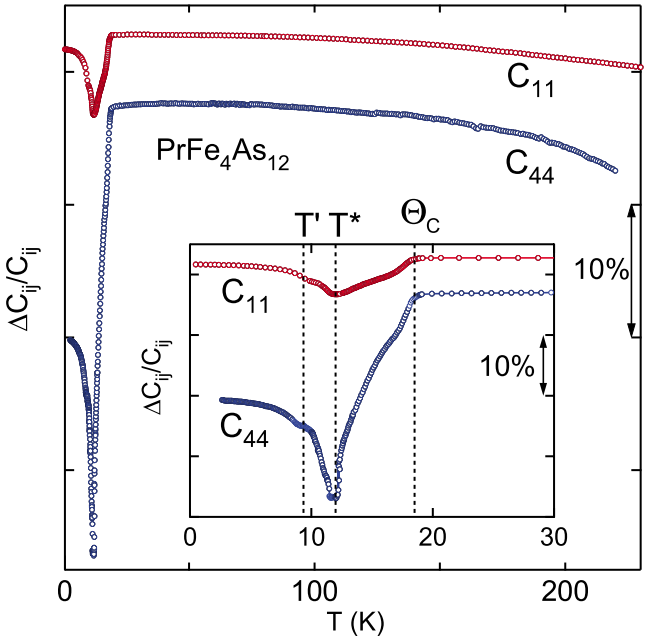

FIG. 11. (Color online) Relative change in the elastic constants $\Delta C_{44}/C_{44}$ and $\Delta C_{11}/C_{11}$ as a function of temperature for $PrFe_4As_{12}$. The inset shows the detailed behavior below 30 K. The vertical dashed lines indicate the characteristic temperatures T', T^*, and Θ_C (see text).

effect, while the C_{11} mode saturates around 30 K. Both the C_{11} and C_{44} modes exhibit a sharp drop near $\Theta_C = 18$ K that are followed by characteristic softenings of 6% and 20%, respectively.

The inset of Fig. 11 shows the detailed behavior of the elastic constants at low temperatures. The vertical dashed lines indicate the three characteristic temperatures, T', T^*, and Θ_C, which are observed in ultrasound measurements. The elastic constants $C_{11}(T)$ and $C_{44}(T)$ display a sharp minimum at $T^* = 12$ K, below which both elastic constants increase with decreasing temperature down to 0.4 K. Another small curvature change is observed at $T' \sim 10$ K in both elastic constants, where the specific heat and ac susceptibility each show a broad maximum. In addition, a considerable deterioration of the ultrasonic echoes (not shown) in both the C_{11} and C_{44} modes occurs for $12 \leq T \leq 18$ K, where the ultrasonic attenuation increases.

The considerable (20%) softening found in C_{44} is proportional to $1/T$ in the range between 18 and 12 K, which can be explained by a Curie–Weiss law of the form $C_{ij} = C_{ij}^0 (T - \Theta)/(T - T_C)$. This Curie-type softening of the C_{44} mode indicates that the CEF ground state of the Pr^{3+} ion has diagonal matrix elements for Γ_5-type quadrupoles. This characteristic softening and the critical attenuation behavior are similar to those of the ferroquadrupolar (FQ) compounds DyB_6 and HoB_6, which show a considerable softening of 70% in the C_{44} mode.[54] The compound PrB_6 also shows a softening of 34% from 400 K down to the magnetic ordering temperature at 7.1 K in the C_{44} mode due to the Γ_5 triplet CEF ground state. However, the ferromagnetic ordering at Θ_C may be accompanied by a local distortion of the Fe_4As_{12} cage, such that a change occurs in the Pr^{3+} ion's CEF environment,

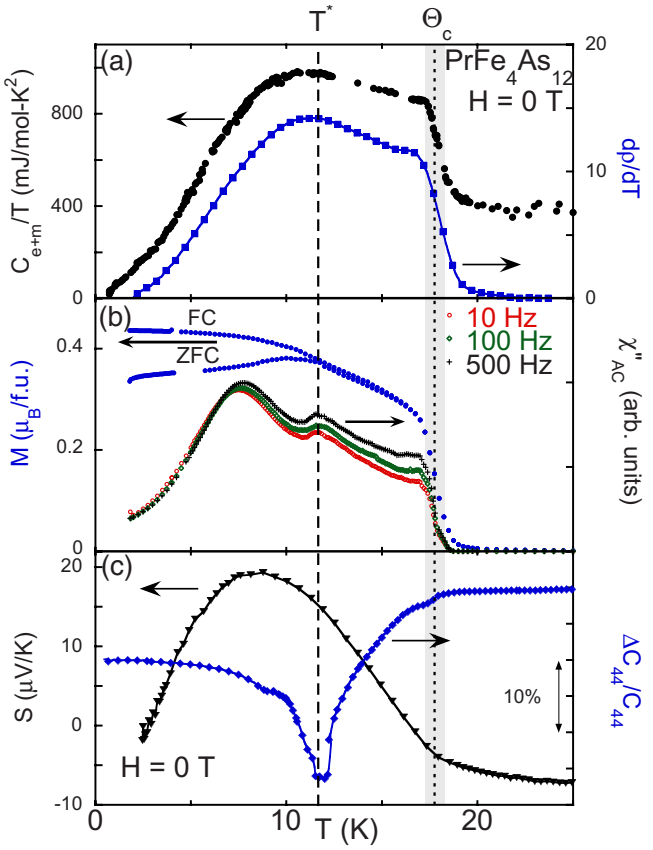

FIG. 12. (Color online) A comparison of low-temperature specific heat, electrical resistivity, magnetization, ac susceptibility, thermopower, and ultrasound data that are used to correlate features that are observed at the ferromagnetic ordering temperature Θ_C (dotted line) and the characteristic temperature T^* (dashed line). (a) Temperature derivative of resistivity and electronic plus magnetic contributions to specific heat, which shows a striking resemblance of the temperature dependence of each throughout the entire range. (b) Low-field (5 mT) dc magnetization and the imaginary part of the ac susceptibility, highlighting the coincidence of both the irreversibility temperature in $M(T)$ and the peak in $\chi''_{ac}(T)$ with T^*. (c) Zero-field thermoelectric power and transverse sound velocity data.

leading to a splitting of the Γ_5 ground state triplet. For this reason, the simple Curie–Weiss softening scenario with a Γ_5 CEF ground state may not be appropriate for the present results for C_{44} of $PrFe_4As_{12}$ unless the ground state accidentally remains degenerate for Γ_5-quadrupole transitions below Θ_C. If the origin of the transition at $T^* = 12$ K is a Γ_5-type FQ transition, a trigonal lattice distortion of $\varepsilon_{yz} = \varepsilon_{zx} = \varepsilon_{xy} \neq 0$ due to the cooperative Jahn–Teller effect is expected. Until neutron scattering or thermal expansion measurements have been performed, however, the possible lattice distortion originating from FQ ordering cannot be established.

IV. DISCUSSION

A direct comparison of several measurements at the characteristic temperatures T^* and Θ_C is presented in Fig. 12 to gain insight into the properties of $PrFe_4As_{12}$. The shaded region at Θ_C (denoting the finite transition width) lines up

with the sharp increases in $C_{e+m}(T)/T$, $d\rho(T)/dT$, $\chi''_{ac}(T)$, and $M(T)$, as shown in Figs. 12(a) and 12(b), and it coincides with the kinks in $S(T)$ and $\Delta C_{44}(T)/C_{44}$ in Fig. 12(c). The temperature T^* (Fig. 12, dashed line), which is defined as the maximum in $\chi''_{ac}(T)$ at 11.7 K [Fig. 12(b)], lies near the broad maximum in $C_{e+m}(T)/T$ and $d\rho(T)/dT$ in Fig. 12(a) and also coincides with both T_{irr} in $M(T)$ and a deep minimum in $\Delta C_{44}(T)/C_{44}$ [Figs. 12(b) and 12(c), respectively]. Although there is no clear feature at T^* in the thermopower, the peak in S near ~ 8 K appears to coincide with a large peak in $\chi''_{ac}(T)$ as well as a kink in $\Delta C_{44}(T)/C_{44}$.

The striking similarity of the derivative with respect to temperature of the electrical resistivity, $d\rho(T)/dT$, and $C_{e+m}(T)/T$, as shown in Fig. 12(a), implies that the transport scattering is dominated by magnetic fluctuations below Θ_C. Fisher and Langer[55] showed that the magnetic specific heat and $d\rho(T)/dT$ are indeed related through the spin-spin correlation function. Although for $PrFe_4As_{12}$, $d\rho(T)/dT$ is similar to $C_{e+m}(T)/T$, rather than $C_m(T)$, this argument may be responsible for their nearly identical behavior if the major contribution to $C_{e+m}(T)$ is $C_m(T)$.

The sharp increases in $\chi''_{ac}(T)$ and in $C_{e+m}(T)/T$ imply an onset of magnetic ordering at Θ_C. This temperature also coincides with additional features, as seen in $M(T)$, $d\rho(T)/dT$, and ultrasound, as highlighted in each data set. For temperatures below Θ_C, a very deep minimum in $\Delta C_{44}(T)/C_{44}$ develops at T^* and is consistent with a structural phase transition, which is possibly a Jahn–Teller distortion: the transition seems to induce (or coincide with) a change in the magnetic ordering. Confirmation of this comes from magnetization measurements along with two different orientations that indicate a change in the magnetic easy axis from [111] at Θ_C to [100] at T^*.

Additionally, this change can be seen in the magnetization through the development of a strong irreversibility at T_{irr} in low fields and a change in the slope of the magnetization at high fields. Possible sources for the observed irreversibility in $M(T)$ and the frequency dependence of $\chi''_{ac}(T)$ are a spin glass behavior or magnetic domains.[30,31,56] The increase in magnitude of $\chi''_{ac}(T)$ with increasing frequency from ~ 7 K to Θ_C is consistent with a glassylike behavior. However, a general spin glass behavior can be ruled out by the behavior of $\chi'_{ac}(T)$, which shows no clear indication of a spin-glass freezing temperature nor does it show any strong dependence on driving frequency. Rather, the observed magnetic anisotropy of $PrFe_4As_{12}$ is consistent with magnetic domains as the source of the irreversibility.[31,33] In this picture, the anisotropy acts as an energy barrier to the magnetic domain alignment that must be overcome—either by an applied field or with increasing temperature.[57] The small magnitude of the irreversibility along with the low fields required to suppress it are consistent with this scenario since a small magnetic anisotropy is expected in cubic $PrFe_4As_{12}$.

To better understand the phase diagram and to confirm the CEF ground state for $PrFe_4As_{12}$, additional measurements of ultrasound and specific heat in finite magnetic fields are planned. In an applied field, the Γ_5 CEF ground state inferred from the saturation moment would be split, leading to Schottky anomalies in the specific heat and a softening of the C_{44} mode in ultrasound. Moreover, specific heat measurements in a field could help determine the nature of the shoulder at $T \approx 10$ K, as well as the field-induced increase in magnon thermal conductivity in the same temperature range. Planned scattering experiments will allow a clear understanding of the magnetic structure that is observed in $PrFe_4As_{12}$, shedding light on the magnetic interactions, and the CEF level scheme. Fe Mössbauer measurements along with x-ray magnetic circular dichroism would also prove helpful by elucidating the contribution of iron to the magnetism and magnetic moment that are observed in $PrFe_4As_{12}$.

V. SUMMARY

Measurements of magnetization, specific heat, electrical resistivity, thermal transport, thermoelectric power, and ultrasound are reported for single crystals of $PrFe_4As_{12}$. Abrupt features that are observed in all measured quantities indicate that ferromagnetic ordering occurs below $\Theta_C = 18$ K. Furthermore, $M(H,T)$ measurements reveal a change in the easy axis at low temperatures, $T < 12$ K, and low fields, $H < 0.8$ T. Additional features that are observed in susceptibility and ultrasound measurements confirm the existence of one or more additional transitions at temperatures below Θ_C, which is possibly associated with a structural change. Whether or not this drives the change in easy axis remains to be established in future studies.

ACKNOWLEDGMENTS

This work was supported by the U.S. Department of Energy under Grant No. DE-FG02-04ER46105 and the U.S. National Science Foundation under Grant No. DMR 0335173. J.P. acknowledges the support from NSERC Canada. Research at Wrocław was supported by the Polish Ministry of Science and Higher Education (Grant No. NN 202 4129 33).

[1] M. B. Maple, E. D. Bauer, N. A. Frederick, P.-C. Ho, W. M. Yuhasz, and V. S. Zapf, Physica B (Amsterdam) **328**, 29 (2003).
[2] Y. Aoki, H. Sugawara, H. Harima, and H. Sato, J. Phys. Soc. Jpn. **74**, 209 (2005).
[3] M. B. Maple, Z. Henkie, W. M. Yuhasz, P.-C. Ho, T. Yanagisawa, T. A. Sayles, N. P. Butch, J. R. Jeffries, and A. Pietraszko, J. Magn. Magn. Mater. **310**, 182 (2007).
[4] M. S. Torikachvili, J. W. Chen, Y. Dalichaouch, R. P. Guertin, M. W. McElfresh, C. Rossel, M. B. Maple, and G. P. Meisner, Phys. Rev. B **36**, 8660 (1987).
[5] Y. Aoki, T. Namiki, T. D. Matsuda, K. Abe, H. Sugawara, and H. Sato, Phys. Rev. B **65**, 064446 (2002).
[6] L. Hao, K. Iwasa, M. Nakajima, D. Kawana, K. Kuwahara, M. Kohgi, H. Sugawara, T. D. Matsuda, Y. Aoki, and H. Sato, Acta

Phys. Pol. B **34**, 1113 (2003).
[7] M. B. Maple, E. D. Bauer, V. S. Zapf, E. J. Freeman, and N. A. Frederick, Acta Phys. Pol. B **32**, 3291 (2001).
[8] E. D. Bauer, N. A. Frederick, P.-C. Ho, V. S. Zapf, and M. B. Maple, Phys. Rev. B **65**, 100506(R) (2002).
[9] M. B. Maple, P.-C. Ho, V. S. Zapf, N. A. Frederick, E. D. Bauer, W. M. Yuhasz, F. M. Woodward, and J. M. Lynn, J. Phys. Soc. Jpn. **71**, 23 (2002).
[10] Y. Aoki, A. Tsuchiya, T. Kanayama, S. R. Saha, H. Sugawara, H. Sato, W. Higemoto, A. Koda, K. Ohishi, K. Nishiyama, and R. Kadono, Phys. Rev. Lett. **91**, 067003 (2003).
[11] K. Izawa, Y. Nakajima, J. Goryo, Y. Matsuda, S. Osaki, H. Sugawara, H. Sato, P. Thalmeier, and K. Maki, Phys. Rev. Lett. **90**, 117001 (2003).
[12] T. Cichorek, A. C. Mota, F. Steglich, N. A. Frederick, W. M. Yuhasz, and M. B. Maple, Phys. Rev. Lett. **94**, 107002 (2005).
[13] P.-C. Ho, N. A. Frederick, V. S. Zapf, E. D. Bauer, T. D. Do, M. B. Maple, A. D. Christianson, and A. H. Lacerda, Phys. Rev. B **67**, 180508(R) (2003).
[14] M. Kohgi, K. Iwasa, M. Nakajima, N. Metoki, S. Araki, N. Bernhoeft, J. M. Mignot, A. Gukasov, H. Sato, Y. Aoki, and H. Sugawara, J. Phys. Soc. Jpn. **72**, 1002 (2003).
[15] D. J. Braun and W. Jeitschko, J. Solid State Chem. **32**, 357 (1980).
[16] I. Shirotani, T. Uchiumi, K. Ohno, C. Sekine, Y. Nakazawa, K. Kanoda, S. Todo, and T. Yagi, Phys. Rev. B **56**, 7866 (1997).
[17] T. Namiki, Y. Aoki, H. Sato, C. Sekine, I. Shirotani, T. D. Matsuda, Y. Haga, and T. Yagi, J. Phys. Soc. Jpn. **76**, 093704 (2007).
[18] T. A. Sayles, W. M. Yuhasz, M. B. Maple, A. Pietraszko, R. Wawryk, and Z. Henkie (unpublished).
[19] W. M. Yuhasz, N. P. Butch, T. A. Sayles, P.-C. Ho, J. R. Jeffries, T. Yanagisawa, N. A. Frederick, M. B. Maple, Z. Henkie, A. Pietraszko, S. K. McCall, M. W. McElfresh, and M. J. Fluss, Phys. Rev. B **73**, 144409 (2006).
[20] M. B. Maple, N. P. Butch, N. A. Frederick, P.-C. Ho, J. R. Jeffries, T. A. Sayles, T. Yanagisawa, W. M. Yuhasz, Songxue Chi, H. J. Kang, J. W. Lynn, Pengcheng Dai, S. K. McCall, M. W. McElfresh, M. J. Fluss, Z. Henkie, and A. Pietraszko, Proc. Natl. Acad. Sci. U.S.A. **103**, 6783 (2006).
[21] Z. Henkie, M. B. Maple, A. Pietraszko, R. Wawryk, T. Cichorek, R. E. Baumbach, W. M. Yuhasz, and P.-C. Ho, Proceedings of the International Conference on New Quantum Phenomena in Skutterudite and Related Systems, Kobe, Japan, 26–30 September 2007 (unpublished).
[22] G. M. Sheldrick, *Program for the Solution of Crystal Structures* (University of Göttingen, Germany, 1985).
[23] G. M. Sheldrick, *Program for Crystal Structure Refinement* (University of Göttingen, Germany, 1987).
[24] E. Bauer, St. Berger, Ch. Paul, M. D. Mea, G. Hilscher, H. Michor, M. Reissner, W. Steiner, A. Grytsiv, P. Rogl, and E. W. Scheidt, Phys. Rev. B **66**, 214421 (2002).
[25] N. P. Butch, W. M. Yuhasz, P.-C. Ho, J. R. Jeffries, N. A. Frederick, T. A. Sayles, X. G. Zheng, M. B. Maple, J. B. Betts, A. H. Lacerda, F. M. Woodward, J. W. Lynn, P. Rogl, and G. Giester, Phys. Rev. B **71**, 214417 (2005).
[26] M. E. Danebrock, C. B. H. Evers, and W. Jeitschko, J. Phys. Chem. Solids **57**, 381 (1996).
[27] W. Schnelle, A. Leithe-Jasper, M. Schmidt, H. Rosner, H. Borrmann, U. Burkhardt, J. A. Mydosh, and Y. Grin, Phys. Rev. B **72**, 020402(R) (2005).
[28] T. D. Matsuda, A. Galatanu, Y. Haga, S. Ikeda, E. Yamamoto, M. Hedo, Y. Uwatoko, T. Takeuchi, K. Sugiyama, K. Kindo, R. Settai, and Y. Ōnuki, J. Phys. Soc. Jpn. **73**, 2533 (2004).
[29] X. C. Kou, R. Grössinger, G. Wiesinger, J. P. Liu, F. R. de Boer, I. Kleinschroth, and H. Kronmüller, Phys. Rev. B **51**, 8254 (1995).
[30] K. Binder and A. P. Young, Rev. Mod. Phys. **58**, 801 (1986).
[31] T. H. Jacobs, K. H. J. Buschow, R. Verhoef, and F. R. de Boer, J. Less-Common Met. **157**, L11 (1990).
[32] K. H. J. Buschow and M. Brouha, J. Appl. Phys. **47**, 1653 (1976).
[33] M. Godinho, G. Bonfait, A. P. Gonçalves, M. Almeida, and J. C. Spirlet, J. Magn. Magn. Mater. **140-144**, 1417 (1995).
[34] C. Mazumdar, R. Nagarajan, L. C. Gupta, B. D. Padalia, and R. Vijayaraghavan, Appl. Phys. Lett. **77**, 895 (2000).
[35] B. Bleaney and R. W. Hill, Proc. Phys. Soc. London **78**, 313 (1961).
[36] L. J. Sundström, in *Handbook on the Physics and Chemistry of Rare Earths*, edited by K. A. Gschneider, Jr. and L. Eyring (North Holland, Amsterdam, 1978), Vol. 1, p. 379.
[37] N. J. Stone, At. Data Nucl. Data Tables **90**, 75 (2005).
[38] E. D. Bauer, A. Ślebarski, N. A. Frederick, W. M. Yuhasz, M. B. Maple, D. Cao, F. Bridges, G. Giester, and P. Rogl, J. Phys.: Condens. Matter **16**, 5095 (2004).
[39] A. Tari, *The Specific Heat of Matter at Low Temperatures* (Imperial College, London, 2003).
[40] S. Watanabe and K. Miyake, J. Phys. Soc. Jpn. **71**, 2489 (2002).
[41] A. Huxley, I. Sheikin, E. Ressouche, N. Kernavanois, D. Braithwaite, R. Calemczuk, and J. Flouquet, Phys. Rev. B **63**, 144519 (2001).
[42] V. H. Tran, P. Rogl, G. André, and F. Bourée, J. Phys.: Condens. Matter **18**, 703 (2006).
[43] S. Süllow, I. Prasad, M. C. Aronson, J. L. Sarrao, Z. Fisk, D. Hristova, A. H. Lacerda, M. F. Hundley, A. Vigliante, and D. Gibbs, Phys. Rev. B **57**, 5860 (1998).
[44] P.-C. Ho, W. M. Yuhasz, N. P. Butch, N. A. Frederick, T. A. Sayles, J. R. Jeffries, M. B. Maple, J. B. Betts, A. H. Lacerda, P. Rogl, and G. Giester, Phys. Rev. B **72**, 094410 (2005).
[45] H. Kontani, J. Phys. Soc. Jpn. **73**, 515 (2004).
[46] P. Thalmeier and B. Lüthi, in *Handbook on the Physics and Chemistry of Rare Earths*, edited by K. A. Gshchneider, Jr. and L. Eyring (North Holland, Amsterdam, 1991), Vol. 14, p. 311.
[47] T. D. Matsuda, A. Galatanu, Y. Haga, S. Ikeda, E. Yamamoto, M. Hedo, Y. Uwatoko, T. Takeuchi, K. Sugiyama, K. Kindo, R. Settai, and Y. Ōnuki, J. Phys. Soc. Jpn. **73**, 2533 (2004).
[48] R. Takke, N. Dolezai, W. Assmus, and B. Lüthi, J. Magn. Magn. Mater. **23**, 247 (1981).
[49] H. M. Rosenberg, *Low Temperature Solid State Physics* (Oxford University Press, London, 1963).
[50] J. Paglione, M. A. Tanatar, D. G. Hawthorn, R. W. Hill, F. Ronning, M. Sutherland, L. Taillefer, C. Petrovic, and P. C. Canfield, Phys. Rev. Lett. **94**, 216602 (2005).
[51] K. Behnia, D. Jaccard, and J. Flouquet, J. Phys.: Condens. Matter **16**, 5187 (2004).
[52] A. Pourret, K. Behnia, D. Kikuchi, Y. Aoki, H. Sugawara, and H. Sato, Phys. Rev. Lett. **96**, 176402 (2006).
[53] N. R. Dilley, E. D. Bauer, M. B. Maple, S. Dordevic, D. N. Basov, F. Freibert, T. W. Darling, A. Migliori, B. C. Chakoumakos, and B. C. Sales, Phys. Rev. B **61**, 4608 (2000).

[54] S. Nakamura, T. Goto, S. Kunii, K. Iwashita, and A. Tamaki, J. Phys. Soc. Jpn. **63**, 623 (1994).
[55] M. E. Fisher and J. S. Langer, Phys. Rev. Lett. **20**, 665 (1968).
[56] D. X. Li and Y. Shiokawa, J. Phys.: Condens. Matter **15**, S2029 (2003).
[57] Z. G. Sun, S. Y. Zhang, H. W. Zhang, and B. G. Shen, J. Alloys Compd. **349**, 1 (2003).